Cream roll-inspired advanced MnS/C composite for sodium-ion batteries: encapsulating MnS cream into hollow N,S-co-doped carbon rolls

DOI:
10.1039/D0NR00626B

Document Version
Accepted author manuscript

Nanoscale

Cream rolls-inspired advanced MnS/C composite for sodium-ion batteries: Encapsulating MnS creams into hollow N, S co-doped carbon rolls

Journal:	*Nanoscale*
Manuscript ID	NR-ART-01-2020-000626
Article Type:	Paper
Date Submitted by the Author:	22-Jan-2020
Complete List of Authors:	Li, Gaojie; Zhongyuan University of Technology Chen, Kongyao; Zhongyuan University of Technology, Center for Advanced Materials Research Wang, Yan-Jie; Zhongyuan University of Technology, Center for Advanced Materials Research Wang, Zhuo; Zhongyuan University of Technology, Center for Advanced Materials Research Cui, Siwen; Zhongyuan University of Technology, Center for Advanced Materials Research Chen, Xueli; Zhongyuan University of Technology, Center for Advanced Materials Research Wu, Zijie; University of Manchester, The University of Manchester Aerospace Research Institute Soutis, Constantinos; University of Manchester, The University of Manchester Aerospace Research Institute Chen, Weihua; Zhengzhou University, College of Chemistry and Molecular Engineering Mi, Liwei; Zhongyuan University of Technology, Center For Advanced Materials Research

Nanoscale

Guidelines for Referees

Thank you very much for agreeing to review this manuscript for *Nanoscale*.

Nanoscale is a high impact international journal, publishing high quality research across nanoscience and nanotechnology. It publishes a full mix of research articles on experimental and theoretical work, including reviews, communications and full papers.

Nanoscale Associate Editors stress very high standards for acceptance in the journal. Articles must report extremely novel, very high quality, reproducible new work of broad general interest.

Nanoscale's Impact Factor is **6.970** (2018 Journal Citation Reports®)

The following manuscript has been submitted for consideration as a

PAPER

For acceptance, papers must report original scientific work that has not been published previously. Full papers do not have a page limit and should be appropriate in length for scientific content.

When preparing your report, please:

- Focus on the **originality**, **importance**, **impact** and **reproducibility** of the science.
- Refer to the **journal scope and expectations**.
- **State clearly** whether you think the article should be accepted or rejected and give detailed comments (with references) both to help the Editor to make a decision on the paper and the authors to improve it
- **Inform the Editor** if there is a conflict of interest, a significant part of the work you cannot review with confidence or if parts of the work have previously been published.
- **Provide your report rapidly** or inform the Editor if you are unable to do so.

Best regards,

Professor Chunli Bai
Editor-in-Chief, *Nanoscale*

Professor Dirk Guldi
Editor-in-Chief, *Nanoscale*

Dr Michaela Muehlberg
Managing Editor, *Nanoscale*

Contact us

Please visit our reviewer hub for further details of our processes, policies and reviewer responsibilities as well as guidance on how to review, or click the links below.

What to do when you review

Reviewer responsibilities

Process & policies

Justification

1. Inspired by the unique structure of common cream rolls, novel MnS/NSCTs composite is prepared via a simple and low-cost method.
2. This cream rolls-like MnS/NSCTs composite delivers the best comprehensive electrochemical performance among all MnS electrodes for sodium-ion batteries until now.
3. The conversion reaction mechanism of MnS/NSCTs is clearly revealed by several *in-situ* and *ex-situ* techniques.

Dear Professor,

Happy new year to you! We would like to submit a research article entitled "**Cream rolls-inspired advanced MnS/C composite for sodium-ion batteries: Encapsulating MnS creams into hollow N, S co-doped carbon rolls**" for your consideration to be published in ***Nanoscale***. I would like to declare on behalf of my co-authors that this work is original research, and has not been published or under consideration for publication elsewhere.

Manganese sulfide (MnS) is a potential anode material for sodium-ion batteries for its high theoretical capacity and low price. However, complicated preparation and limited practical capacity still hinder the application, so more efforts should be taken. Inspired by the unique structure of cream rolls, MnS/N, S co-doped carbon tubes (MnS/NSCTs) composite with 3D cross-linked tubular structure is prepared via a simple and low cost method in this work. More importantly, this cream rolls-like MnS/NSCTs composite delivers the best electrochemical performance until now (the highest capacity of 550.6 mA h g^{-1} at 100 mA g^{-1}, the highest capacity of 447.0 mA h g^{-1} after 1400 cycles at 1000 mA g^{-1}, and the best rate performance of 319.8 mA h g^{-1} at 10000 mA g^{-1}) when act as anode for sodium-ion batteries. Besides, according to several *in-situ* and *ex-situ* techniques, the conversion reaction mechanism of MnS/NSCTs is clearly revealed, and the superior electrochemical performance can be attributed to the unique cream roll-like structure. The preparation of MnS/NSCTs is feasible for other anode materials, which will greatly promote the development of sodium-ion batteries.

Thank you very much for your kind consideration. Happy new year to you again!

Yours sincerely,

Liwei Mi

ARTICLE

Cream rolls-inspired advanced MnS/C composite for sodium-ion batteries: Encapsulating MnS creams into hollow N, S co-doped carbon rolls

Received 00th January 20xx,
Accepted 00th January 20xx

DOI: 10.1039/x0xx00000x

Gaojie Li,[a] Kongyao Chen,*[a] Yanjie Wang,[a] Zhuo Wang,[a] Xueli Chen,[a] Siwen Cui,[a] Zijie Wu,[a,c] Constantinos Soutis,[c] Weihua Chen,*[b] Liwei Mi*[a]

With advantages of high theoretical capacity and low cost, manganese sulfide (MnS) becomes a potential electrode material for sodium-ion batteries (SIBs). However, complicated preparations and limited cycle life still hinder its application. Inspired by cream rolls in our daily life, MnS/N, S co-doped carbon tubes (MnS/NSCTs) composite with 3D cross-linked tubular structure is prepared via an ultra-simple and low cost method in this work. As anode for SIBs, the cream rolls-like MnS/NSCTs composite delivers the best electrochemical performance until now (the highest capacity of 550.6 mA h g^{-1} at 100 mA g^{-1}, the highest capacity of 447.0 mA h g^{-1} after 1400 cycles at 1000 mA g^{-1}, and the best rate performance of 319.8 mA h g^{-1} at 10000 mA g^{-1}). Besides, According to several *in-situ* and *ex-situ* techniques, the sodium storage mechanism of MnS/NSCTs is mainly made of conversion reaction, and the superior electrochemical performance of MnS/NSCTs is mainly attributed to the unique cream roll-like structure. More importantly, this simple method may be feasible for other anode materials, which will greatly promote the development of SIBs.

Introduction

In recent years, sodium-ion batteries (SIBs) have been considered one of the most competitive candidates for electrochemical energy storage system, due to their abundant resources, low price, environmental protection and hypotoxicity[1-4]. However, few insertion sites, high insertion barrier, sluggish insertion kinetics of sodium ions, and poor structural stability of common electrodes seriously hinder the development of SIBs[5-8]. Many researchers have attempted to improve the performance of the electrodes through nano-crystallization, doping/compound modification and electrode/battery structure optimization, which has already achieved a series of remarkable achievements[9-12].

Nowadays, anode materials for SIBs mainly include carbonaceous materials, metal oxides/sulfides, alloy materials, and organic compounds[13-18]. Among them, metal sulfides have been deemed as potential candidates in consideration of their high theoretical capacities, abundant resources and hypotoxicity[19-22]. Nevertheless, some important disadvantages such as large volume change, rapid capacity fading and inferior conductivity need to be addressed before application[23-25]. Among various metal sulfides, MnS is a semiconductor with a wide bandwidth of 3.7 eV. According to the structure differences, MnS can be divided into three different types (α, β and γ, respectively). Among them, α-MnS is a green rock-salt crystal with the best thermostability, and β-MnS and γ-MnS are red crystals with sphalerite and wurtzite structure respectively[26]. In previous research, MnS is usually applied to powder metallurgy, magnetic semiconductors and photoelectricity. However, in consideration of the high theoretical capacity (660 mA h g^{-1}) and good structure stability, MnS may be a potential long-life electrode for SIBs. In recent years, the sodium storage performance of MnS was preliminarily explored[27, 28]. For example, hollow α-MnS/RGO microspheres, which were prepared via a hydrothermal method, showed a high initial capacity (497 mA h g^{-1}) and a proper cycle life (308 mA h g^{-1} after 125 cycles)[29]. α-MnS/carbon fiber composites, which were prepared by electrospinning technique, showed a stable capacity of 220 mA h g^{-1} after 200 cycles[29]. Besides, C-α-MnS exhibited an initial capacity of 302 mA h g^{-1} and a retention of 86% after 200 cycles. What's more, the sodium storage mechanism of MnS was also studied by several *ex-situ* techniques, and the conversion reaction mechanism was preliminarily proposed[30]. Based on previous reports, MnS shows potential application in SIBs, but the capacity and rate performance of MnS should be further improved[26]. Besides, complex, expensive and pollutional methods will also hinder the large-scale application of MnS in SIBs.

To address these problems, many efforts should be taken to develop low-cost and green preparation of MnS electrode. Besides, construction of 3D conductive MnS/C composites, which MnS nanoparticles are located into carbon matrix, is also very important to improve the electrochemical performance. Then green biological template methods may be suitable solutions. In related reports, various biomass carbon materials have gained our attention for their green, renewable and low cost merits. Besides, most biomass carbon materials can inherit complex microstructures from their precursors, then the structure stability of metal sulfides/biomass carbon composites can be improved[31-33]. Moreover, rich heteroatoms (N, S

[a] Center for Advanced Materials Research, Zhongyuan University of Technology, Henan 450007, P. R. China; E-mail: mlwzzu@163.com, chenweih@zzu.edu.cn
[b] College of Chemistry and Molecular Engineering, Zhengzhou University, Henan 450001, P. R. China. E-mail: chenweih@zzu.edu.cn
[c] The University of Manchester Aerospace Research Institute, University of Manchester, Manchester M13 9PL, United Kingdom
Electronic Supplementary Information (ESI) available: [details of any supplementary information available should be included here]. See DOI: 10.1039/x0xx00000x

and so on) in the microstructure of biomass carbon will further improve the conductivity and sodium storage activity. Among various biomass materials, juncus is a cheap natural herb with 3D cross-linked tubular structure. And this specific structure can be well maintained in its biomass carbon derivative. What's more, this cross-linked carbon shows good structure stability, electronic conductivity and corrosion resistance[33, 34].

As a kind of delicious and popular dessert, cream rolls could be found everywhere in our daily life. Most cream rolls are made of external hollow rolls and internal creams, and soft creams are well encapsulated and protected by stable rolls. In this way, creams can keep stable, and the rolls become more delicious. Inspired by the structure similarity between cream rolls and natural herb juncus, we propose an ultra-simple method to prepare high-performance MnS/C electrodes. Specifically, high-capacity but unstable MnS particles are well encapsulated into stable N, S co-doped carbon tubes, forming a unique cream roll-like structure. According to several *in-situ* and *ex-situ* mechanism studies, the sodium storage process of MnS/NSCTs is mainly made of conversion reaction. Besides, the impedance of MnS shows good reversibility with the assistance of carbon tubes. Among all the MnS anodes for SIBs, MnS/NSCTs composite in this work delivers the best electrochemical performance. MnS/NSCTs composite shows the highest capacity of 550.6 mA h g^{-1} at 100 mA g^{-1}, and delivers the highest capacity of 447.0 mA h g^{-1} at 1000 mA g^{-1}after 1400 cycles. What's more, MnS/NSCTs composite also shows a capacity of 319.8 mA h g^{-1} at 10000 mA g^{-1}, exhibiting the best rate performance. More importantly, this simple and low cost method may be feasible for other anode materials, which will greatly promote the development of SIBs.

Results and discussion

The construction process of cream roll-like MnS/NSCTs composite can be revealed by SEM (Fig. 1). To be specific, pure MnS sample is composed of many uneven aggregates (5~40 μm) which are all made of uneven MnS particles (Fig. 1a). Generally speaking, serious agglomeration of MnS particles will seriously obstruct the Na^+ insertion and electron transport, leading to inferior electrochemical performance. Inspired by the unique structure of cream rolls, cross-linked carbon tubes derived from juncus are considered as suitable shells, and cream-like MnS particles can be encapsulated in the shells. As is shown in Fig. 1b, this biomass carbon can inherit the cross-linked tubular structure from juncus after carbonized in inert atmosphere. The carbon tubes are made of round/oval carbon tubes with interior diameters of 2~4 μm, and the thickness of the tubes is about 0.5 μm. Besides, the internal surface is really rough (the insert of Fig. 1b), which may provide a lot of load sites for MnS particles.

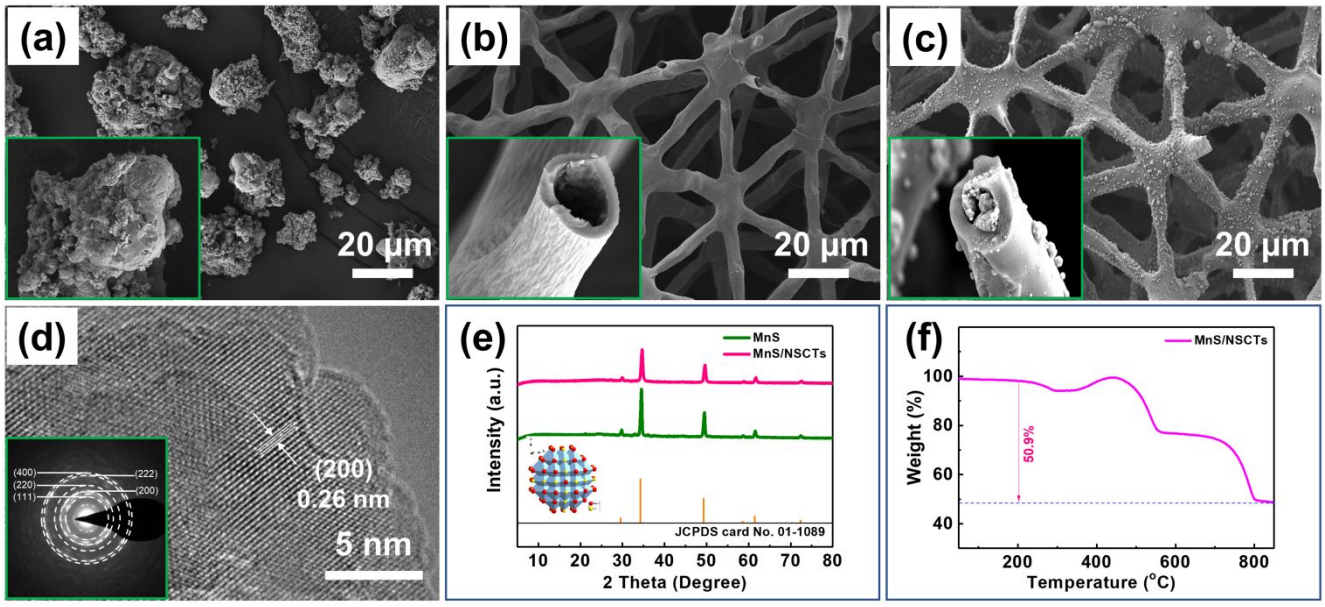

Fig. 1 Morphologies of the samples. (a) SEM image of MnS; (b) SEM image of the carbon tubes; (c) SEM image of MnS/NSCTs; (d) TEM image and SAED of MnS/NSCTs; (e) XRD patterns; (f) TG curves.

During the experiments, we found that manganese nitrate solution could be spontaneously absorbed into the tubes via capillary action. This nature is the key to realize the encapsulation of MnS particles. In addition, samples from the freeze drying method show better uniformity than those from the heat drying method. Therefore, cream roll-like MnS/NSCTs samples are prepared via an ultra-simple method, which includes immersion, freeze drying and heat-treatment processes. The obtained MnS/NSCTs sample shows similar microstructure with carbon tubes, and cross-linked tubular structure is well maintained (Fig. 1c). What's more, the interior cavities of the tubes are filled with many small particles, but few particles are distributed on the surface (the insert of Fig. 1c). This unusual phenomenon may be attributed to the powerful capillary action of juncus. Specifically, manganese acetate solution is mainly absorbed into the interior of the tubes during the initial immersion process, and a large number of MnS particles will be produced in the interior of the tubes during the following freeze drying and heat-treatment processes. On the other hand, little solution is absorbed on the external surface of the tubes, then few MnS particles are produced. This unique cream roll-like structure will be conducive to mitigate the volume expansion of MnS particles during Na^+ insertion process, and further improve the structure stability of MnS/NSCTs electrodes. The high-resolution TEM image shows an interplanar spacing of 0.26 nm, corresponding to (200) plane of cubic MnS (Fig. 1d). Besides, selected area electron diffraction (SAED) results show an obvious polycrystalline feature, and the diffraction rings can be

attributed to (111), (200), (220), (222) and (400) planes of cubic MnS (the insert of Fig. 1d).

XRD patterns of MnS and MnS/NSCTs samples are shown in Fig. 1e. For pure MnS, six strong diffraction peaks appear at 29.6°, 34.3°, 49.3°, 58.6°, 61.4° and 72.3°, which can be attributed to (111), (200), (220), (311), (222) and (400) planes of cubic MnS (JCPDF 01-0891), respectively[30]. In addition, no diffraction peak of other phases appears, indicating high purity. On the other hand, MnS/NSCTs sample shows similar but weaker diffraction peaks, which may result from good encapsulation of MnS by carbon tubes. XRD results demonstrate the feasibility of this method. According to the BET results (Fig. S2a), the specific surface area of MnS/NSCTs is about 36.05 $m^2 g^{-1}$, and the average porous size is 3.74 nm. Besides, the weight ratio of MnS is about 56.0% in the cream roll-like MnS/NSCTs sample (Fig. 1f).

In order to further determine the element ratio and distribution in MnS/NSCTs composites, EDS test is implemented. As is shown in Fig. S1a, the atomic ratio of Mn, S, C and N is 15.94:21.68:58.19:4.64. The EDS result proves the co-existence of MnS and doped S in the composite. Based on the EDS result, the weight ratio of MnS, S, N and C is about 58.3:8.6:2.9:30.2, which is consistent with TG result. What's more, element mapping results reveal that Mn, S, C and N are evenly distributed in the tubular structure (Fig. S1). The above results reveal that MnS "creams" are spontaneously capsulated into N, S co-doped carbon "rolls", and that cream roll-like MnS/NSCTs composites are achieved.

The surface chemical composition of MnS/NSCTs is analyzed by XPS. The survey spectrum demonstrates the presence of Mn, S, C, N and O (Fig. S2b), and O element may come from the surface oxidation of the sample in the air. XPS spectrum of Mn 2p is shown in Fig. S2c, and the curve can be divided into three peaks. The peaks at 641.7 eV and 653.6 eV belong to Mn $2p_{3/2}$ and Mn $2p_{1/2}$ of MnS, respectively. Besides, the peaks at 640.1 and 645.2 eV may be attributed to the multiple splitting of energy levels of Mn ion, indicating chemical bonding between MnS and carbon[35]. The XPS spectrum of S 2p is composed of several peaks (Fig. S2d), which are located at 160.9 eV (S $2p_{3/2}$ of MnS), 162.1 eV (S $2p_{1/2}$ of MnS), 163.9 eV (S $2p_{3/2}$ of S) and 165.0 eV (S $2p_{1/2}$ of S), respectively[36, 37]. In addition, the peak at 168.8 eV may belong to sulfates on the surface. The XPS spectrum of S demonstrates the existence of S in carbon tubes, which may come from high-temperature sulfuration process. The XPS spectrum of C1s can be divided into two peaks at 284.6 eV and 285.8 eV, corresponding to C-C/C-S and C-N/C-O, respectively (Fig. S2e)[38]. In Fig. S2f, the XPS spectrum of N1s can be divided into two peaks. The peak at 398.7 eV belongs to pyridinic-N, and the peak at 400.8 eV belongs to pyrrolic-N. Besides, the peak at 398.7 eV belongs to oxidized-N. Element N, which comes from juncus precursor, can improve the electronic conductivity of carbon tubes[39]. XPS results demonstrate that MnS/NSCTs sample is mainly composed of MnS and N, S co-doped carbon tubes.

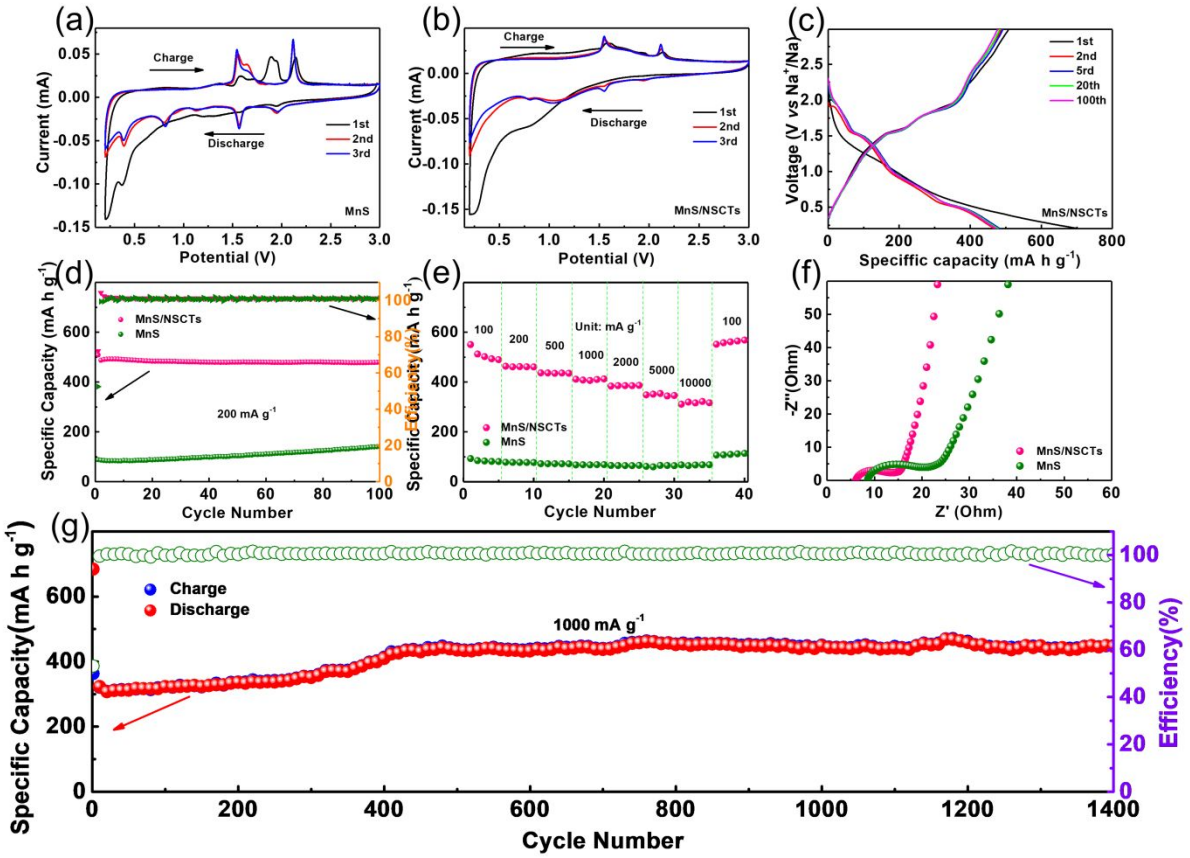

Fig. 2 Electrochemical performance of the samples (the voltage range is 0.2~3.0 V, and the specific capacities are based on the weight of MnS or MnS/NSCTs samples). (a) CV curves of MnS; (b) CV curves of MnS/NSCTs; (c) charge-discharge profiles of MnS/NSCTs; (d) cycle contrast; (e) rate contrast; (f) EIS contrast; (g) long cycle performance of MnS/NSCTs.

The sodium storage behaviors of MnS and MnS/NSCTs are evaluated by CR-2032 coin cells. The CV curves of MnS are shown in Fig. 2a. During the initial reduction process, no obvious peaks appear in high voltage range. Subsequently, two sharp reduction peaks at 0.40 V and 0.20 V may be attributed to the dramatic conversion reaction, then metallic Mn and Na-S compounds are generated[30]. As for the initial oxidation process, several oxidation peaks at 1.60 V, 1.90 V and 2.15 V may correspond to the multi-step conversion reaction. The subsequent CV curves are slightly different from the first ones. Firstly, two reduction peaks at 1.53 V and 0.62 V become clear, but the oxidation peak at 1.90 V disappears. Besides, the reduction peaks at 0.40 V and 0.20 V become weaker, but the oxidation peaks at 1.60 V, 1.70 V and 2.15 V become stronger. For MnS/NSCTs, two broad peaks appear at 0.80 V and 0.20 V during the first reduction process (Fig. 2b). During the first oxidation process, three weak peaks appear at 1.53 V, 1.90 V and 2.11 V, respectively. The CV curves of MnS/NSCTs are similar but more stable than MnS, indicating a more reversible sodium storage process. Fig. 2c shows the charge-discharge profiles of MnS/NSCTs. Specifically, the initial discharge curve is made up of a long sloping line. Subsequently, three short platforms appear at 1.6 and 2.0 V in the charge curve. During the following cycles, the discharge and charge curves are all composed of several short platforms. In general, the charge-discharge curves of MnS/NSCTs match well with the CV curves. Besides, the charge-discharge curves overlap with each other, indicating an excellent electrochemical reversibility of MnS/NSCTs.

In order to confirm the promotion effect of carbon networks to MnS, cycle performance of MnS and MnS/NSCTs is compared with each other. As is shown in Fig. 2d, MnS exhibits a low initial capacity (88.3 mA h g^{-1}) and a low coulombic efficiency (52.5%) at 200 mA g^{-1}. After 100 cycles, the specific capacity of MnS increases to 141.2 mA h g^{-1}, indicating a stable structure cyclicity but low capacity. The poor capacity of MnS may stem from serious agglomeration of MnS particles, then Na^+ can hardly insert into the bulks. On the other hand, cream roll-like MnS/NSCTs composite shows high initial charge capacity (508.9 mA h g^{-1} at 200 mA g^{-1}) and coulombic efficiency (72.1%). After 100 cycles, the capacity retention of MnS/NSCTs still maintains 479.4 mA h g^{-1}. Furthermore, the coulombic efficiency rapidly rises to almost 100% in the following cycles, exhibiting a superior electrochemical reversibility. According to the morphology analysis of MnS/NSCTs after 100 cycles (Fig. S3a-b), most of the cross-linked tubes remain the same. Besides, the cross-section image manifests that the tube is still filled with MnS particles, and that only few particles are found on the surface. Furthermore, many small holes appear on the surface of the tubes, which may result from repeated insertion/extraction process of Na^+. On the other hand, the element distribution in the tube is studied by line scan and element mapping (Fig. S3c). The line scan results show that the shell is mainly composed of carbon, and that the filler is mainly composed of Mn and S, indicating stable cream roll-like structure. Besides, the mapping results match well with the line scan, and MnS particles are still well encapsulated by carbon tubes after 100 cycles (Fig. S3d-f).

The existence of carbon tubes can also improve the rate performance of MnS. In contrast, pure MnS shows low capacities of 93.2, 78.2, 72.3, 67.6, 65.4, 61.7, 64.5 mA h g^{-1} at current densities of 100, 200, 500, 1000, 2000, 5000 and 10000 mA g^{-1}, respectively (Fig. 2e). However, with the assistance of carbon tubes networks, nano-sized MnS particles are well protected via physical encapsulation and chemical absorption, then MnS/NSCTs shows much higher capacities of 550.6, 463.8, 436.9, 411.6, 384, 348.7 and 319.8 mA h g^{-1}, respectively. Electrochemical impedance tests also demonstrate the ultra-low impedance of MnS/NSCTs electrode (Fig. 2f).

In order to investigate the long-term structure stability of MnS/NSCTs, a long cycle test is performed at a current density of 1000 mA g^{-1}. As is shown in Fig. 2g, MnS/NSCTs shows an initial capacity of 363.1 mA h g^{-1}. Besides, a slight capacity increase phenomenon appears during the initial cycles, which is a common activation phenomenon in metal oxides and sulfides[40, 41]. According to previous reports, the activation process is made of continuous particle pulverization and reconstruction process, and new sodium storage sites appear during the electrochemical milling process[42]. During the following cycles, MnS/NSCTs shows excellent cycle stability, and the capacity of MnS/NSCTs still remains 448.2 mA h g^{-1} after 1400 cycles.

Table 1. Electrochemical performance contrast of recent MnS electrodes for SIBs.

Samples	Specific Capacity (mA h g^{-1})	Capacity Retention (mA h g^{-1})	Rate Capability (mA h g^{-1})	Ref.
MnS/RGO	497.0 (100 mA g^{-1})	308.0 after 125 cycles (100 mA g^{-1})	118.0 (800 mA g^{-1})	43
C-α-MnS	302.0 (61 mA g^{-1})	272.0 after 200 cycles (61 mA g^{-1})	226.0 (6100 mA g^{-1})	30
MnS/C	296.2 (50 mA g^{-1})	148.3 after 5000 cycles (1000 mA g^{-1})	143.1 (2500 mA g^{-1})	44
MnS@CNF	220.4 (20 mA g^{-1})	220.0 after 200 cycles (20 mA g^{-1})	87.0 (1000 mA g^{-1})	29
MnS/NSCTs	550.6 (100 mA g^{-1})	447.0 after 1400 cycles (1000 mA g^{-1})	311.0 (10000 mA g^{-1})	This work

Recent researches on MnS electrodes for SIBs are shown in Table 1, and most reports focus on MnS/C composites. Compared with other reports, MnS/NSCTs in this work shows the highest specific capacity (550.6 mA h g^{-1} at 100 mA g^{-1}), the longest cyclicity (447.0 mA h g^{-1} after 1400 cycles at 1000 mA g^{-1}) and the best rate performance (319.8 mA h g^{-1} at 10000 mA g^{-1}). The superior electrochemical performance of MnS/NSCTs is attributed to the unique cream roll-like structure. According to the contrast between MnS and MnS/NSCTs, the introduction of cross-linked carbon tubes plays a key role to improve the electrochemical performance of MnS. To be specific, carbon tubes inherit cross-linked tubular structure from juncus, and provide abundant attachment points and inner cavities for MnS. During the preparation process, MnS particles are well encapsulated into carbon tubes through capillary action, which effectively prevents the agglomeration of MnS particles. During the charge-discharge process, cream roll-like MnS/NSCTs sample shows several advantages. Firstly, the introduction of carbon tubes can effectively improve the dispersity of MnS “creams” and provide efficient conductive networks, then the diffusion pathway of ion/electron will be much shorter. Secondly, MnS particles are well immobilized in carbon tubes by physical encapsulation and chemical absorption, then the volume change and sulfides loss will be alleviated. Thirdly, co-doped S and N can provide more sodium storage sites and enhance the conductivity of carbon tubes, then the specific capacity and rate performance of MnS will be largely improved.

Apart from the electrochemical performance improvement, sodium storage mechanism is also a research priority of MnS. In this

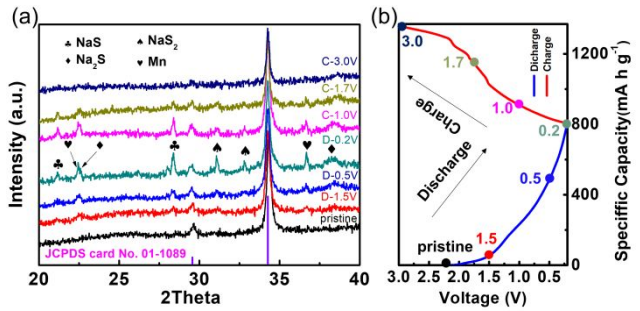

Fig. 3 Crystal structure evolution of MnS/NSCTs during the sodium storage process. (a) ex-situ XRD patterns; (b) corresponding charge-discharge profiles.

work, the sodium storage process is revealed by several *ex-situ* and *in-situ* methods. Based on the crystal structure analysis (the insert of Fig. 1e), MnS belongs to the *Fm3m* space group, and no sites may be available for insertion reaction[45]. Besides, it is hard to achieve Na-Mn alloy from the reaction between Na and Mn[30]. Therefore, the sodium storage process of MnS may relate to the conversion reaction. In order to determine the structure evolution of MnS/NSCTs during the charge-discharge process, *ex-situ* XRD is performed (Fig. 3). For the pristine sample, only diffraction peaks of MnS are detected. During the following sodium storage process, all the peak intensities of MnS decrease gradually. Besides, several new peaks of Mn and NaS appear when discharged to 1.5 V. When discharged to 0.5 V, the conversion reaction further develops, and the diffraction peaks of Na_2S and NaS_2 are detected. When discharged to 0.2 V, the peak intensities of Mn and Na-S compounds further increase. During the following charge process, the peak intensities of Mn and Na-S compounds gradually decrease and eventually disappear, which results from the constant consumption of conversion reaction. Besides, the peak intensities of newly formed MnS are still weak, indicating poor crystallinity. According to the *ex-situ* XRD results, neither insertion reaction nor alloy reaction happens, and only conversion reaction is detected. Therefore, the sodium storage mechanism of MnS can be summarized as follows:

$$3MnS + Na^+ + e^- \rightarrow 2MnS + Mn + NaS \quad (1)$$

$$2MnS + NaS + 2Na^+ + 2e^- \rightarrow 2Mn + Na_2S + NaS_2 \quad (2)$$

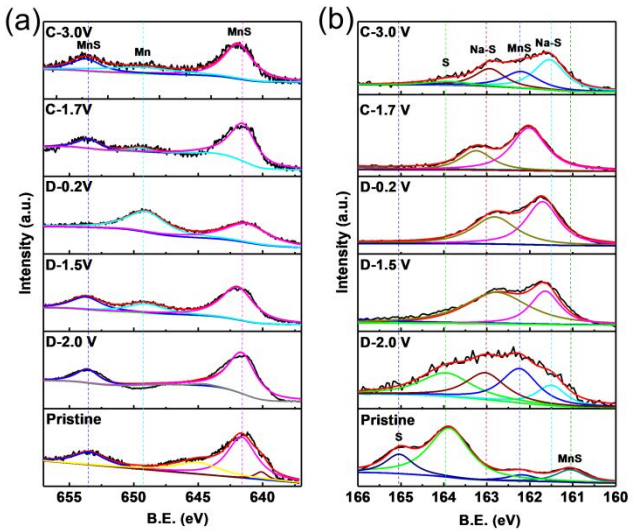

Fig. 4 Chemical component evolution of MnS/NSCTs during the sodium storage process. (a) XPS spectrum of Mn; (b) XPS spectrum of S.

The proposed electrochemical mechanism of MnS is further verified by *ex-situ* XPS (Fig. 4). According to previous, when discharged to 2.0 V, the peaks at 641.7 eV and 653.5 eV belong to Mn $2p_{3/2}$ and Mn $2p_{1/2}$ of MnS, the peaks at 161.4 eV and 162.2 eV belong to S $2p_{3/2}$ and S $2p_{1/2}$ of MnS, and the peaks at 163.0 eV and 163.9 eV belong to S $2p_{3/2}$ and S $2p_{1/2}$ of S[35, 46]. When discharged to 1.5 V, a new peak of Mn^0 (649.5 eV) appears, which may come from the reaction between Na^+ and MnS[47, 48]. On the other hand, two new peaks of Na-S compounds (161.6 eV and 162.8 eV) appear. When discharged to 0.2 V, the reaction between MnS and Na^+ continues. The peak intensity of Mn^0 becomes stronger. Besides, one peak of MnS (653.3 eV) disappears, and another (641.6 eV) becomes weaker. On the other hand, the peaks of Na-S compounds (161.6 eV and 162.8 eV) become stronger[49]. During the following charge process, the peak of Mn^0 (649.5 eV) and Na-S compounds (161.6 eV and 162.8 eV) becomes weaker, but the peaks of MnS (653.3 eV, 641.6 eV and 162.0 eV) appear again[50]. When charged to 3.0 V, the two peaks of MnS move to 653.7 eV and 641.9 eV, which match well with the pristine result. On the other hand, the S2p spectrum is mainly made up of MnS and Na-S compounds. The XPS results demonstrate the conversion reaction between MnS and Na^+, matching well with the *ex-situ* XRD result. However, it's a pity that NaS, Na_2S and NaS_2 can hardly be distinguished via XPS, so more efforts should be done in the future.

Except for structure and chemical composition, impedance evolution can also reflect the electrochemical process of SIBs[48]. However, *in-situ* EIS is barely used in metal sulfides electrodes. *In-situ* EIS test is carried out for the first time to monitor the sodium storage kinetics of MnS. Nyquist-plots at different voltages are shown in Fig. 5. The diagonal in low frequency belongs to the solid-state diffusion resistance (Rs) of sodium ions, and the semicircle in high frequency belongs to the charge-transfer resistance (Rct) across the interface of the electrode[51]. During the whole charge-discharge process, Rs keeps almost unchanged (from 8.8 Ω to 8.5 Ω), manifesting a very stable electrode and battery structure. During the initial discharge process (from 3.0 V to 0.7 V), the Nyquist-plots are all made up of one semicircle and one diagonal, indicating a single-phase sodium storage process. Besides, the R_{ct} decreases gradually from 7.1 Ω to 3.3 Ω, indicating an increasing easy process. However,

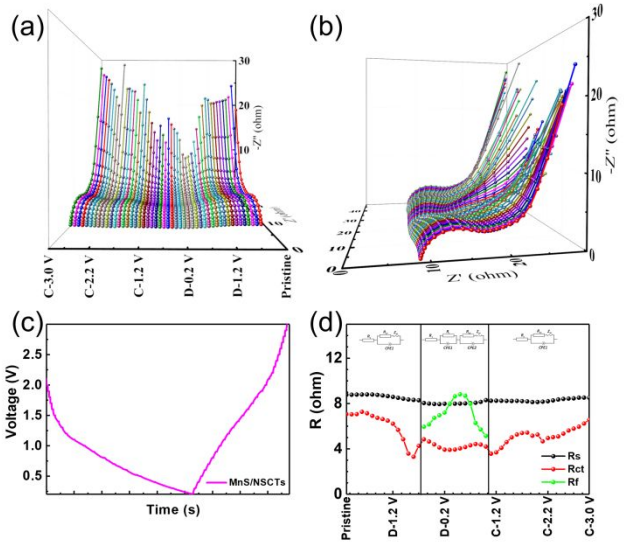

Fig. 5 EIS evolution of MnS/NSCTs during the sodium storage process. (a) (b) EIS curves evolution; (c) corresponding charge-discharge profiles; (d) resistance value evolution according to equivalent circuit fitting.

the Nyquist-plots gradually split into two semicircles and one diagonal (from 0.6 V to 0.2 V and from 0.2 V to 1.0 V), indicating a different multi-phase electrochemical process. The preliminary R_{ct} keeps stable (from 4.9 Ω to 4.2 Ω) during this process. Besides, a new Rct increases from 6.0 Ω to 8.8 Ω at first (from 0.6 V to 0.2 V and from 0.2 V to 0.5 V), then decreases from 8.8 Ω to 5.1 Ω (from 0.5 V to 1.0 V). When charged to 1.1 V, the Nyquist-plots return to one semicircles and one diagonal, indicating a single-phase process which is similar to the original state[39]. Besides, the preliminary R_{ct} increases from 3.6 Ω to 6.6 Ω (from 1.1 V to 3.0 V). In general, the discharge process of MnS/NSCTs is made of two different impedance-evolution models, and the main structure evolution happens in the low voltage range (below 1.0 V). The evolution of the resistance value also reveals a good electron/ion transport reversibility in MnS/NSCTs.

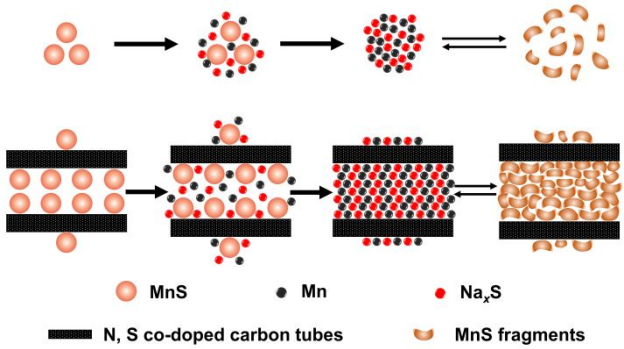

Fig. 6 Micro-structure evolution contrast between MnS and MnS/NSCTs during the sodium storage process.

According to comprehensive analysis of *ex-situ* XRD, *ex-situ* XPS and *in-situ* EIS, with the assistance of N, S co-doped carbon tubes, MnS/NSCTs shows a clear conversion type sodium storage process, accompanied by reversible impedance evolution process, and reversible reaction between MnS, Mn and Na-S compounds. As is shown in Fig. 6, N, S co-doped carbon tubes provides loading sites for MnS particles, thus improve their dispersity and provide efficient conductive networks. Besides, volume change and sulfides loss will be alleviated by efficient encapsulation of carbon tubes. What's more, co-doped S and N can enhance the conductivity of MnS, and provide more active sites. First, the introduction of carbon tubes can effectively improve the dispersity of MnS "creams" and provide efficient conductive networks, then the diffusion pathway of ion/electron will be much shorter. Secondly, MnS particles are well immobilized in carbon tubes by physical encapsulation and chemical absorption, then the volume change and sulfides loss will be alleviated. Thirdly, co-doped S and N can provide more sodium storage sites and enhance the conductivity of carbon tubes, then the specific capacity and rate performance of MnS will be largely improved.

To further reveal the electrochemical kinetic process of MnS/NSCTs, CV curves at different scan rates are performed (Fig. S4a). On the whole, all the peaks become stronger with the increasing scan rates. In addition, CV curves at different scan rates display similar shapes and positions, demonstrating low polarization during the electrochemical process. According to previous reports, the relationship between response current (*i*) and scan rate (*v*) can be concluded from the CV curves[42, 52].

$$i = av^b \quad (3)$$

$$lgi = blgv + lga \quad (4)$$

Herein, *a* and *b* stand for two adjustable parameters. Equation 4 is derived from Equation 3 through a simple mathematical transformation. The *b*-value indicates the capacitive behavior, which can be obtained from the slope of the lg*i*-lg*v* plots. When the *b*-value is 1, the sodium storage process of MnS/NSCTs is a capacitance-controlled process. When the *b*-value is 0.5, the sodium storage process is a diffusion-controlled process. Based on the CV curves, the relationship between log (*i*) and log (*v*) is shown in Fig. S4b, and the *b*-value is 0.709. The capacity contribution of capacitance-controlled process at different scan rates can be quantitatively calculated[53, 54].

$$i = k_1 v + k_2 v^{1/2} \quad (5)$$

Due to the similar CV curves, k_1–value and k_2–value are constant during different scan rates, and $k_1 v$ and $k_2 v^{1/2}$ stand for capacitive contribution and diffusion-controlled process, respectively. The CV curve of MnS/NSCTs at 1.2 mV s^{-1} is shown in Fig. S4c, and most of the integral area is attributed to the capacitive behavior (74.8%). When the scan rates are 0.2, 0.4, 0.6, 0.8 1.0 and 1.2 mV s^{-1}, the capacitive contribution is 49.2%, 52.6%, 57.1%, 61.1%, 65.2% and 74.8%, respectively (Fig. S4d). In general, the capacitive contribution increases with the increasing scan rates. The capacitive behavior of MnS/NSCTs may result from the even distribution of MnS particles in carbon tubes, which results fast transfer of Na^+ and electrons. Actually, the major capacitive behavior will improve the electrochemical kinetics of MnS, which will benefit the electron/ion transports and result in superior rate performance.

Conclusions

In summary, inspired by cream rolls in our daily life, MnS/NSCTs composite with 3D cross-linked tubular structure is designed and prepared via an ultra-simple and low cost method. According to several *in-situ* and *ex-situ* mechanism studies, the sodium storage process of MnS/NSCTs is mainly made of conversion reaction. As anode materials for SIBs, MnS/NSCTs composite delivers the highest capacity of 550.6 mA h g^{-1} at 100 mA g^{-1}. At a current density of 1000 mA g^{-1}, MnS/NSCTs delivers the highest capacity of 447.0 mA h g^{-1} after 1400 cycles. What's more, MnS/NSCTs also shows a capacity of 319.8 mA h g^{-1} at 10000 mA g^{-1}, exhibiting the best rate performance until now. The superior electrochemical performance of MnS/NSCTs is attributed to the unique cream roll-like structure. Firstly, cross-linked carbon "shells" can effectively improve the dispersity of MnS particles and provide efficient conductive networks for ion/electron transfer. Secondly, MnS "creams" are well immobilized in carbon tubes by physical encapsulation and chemical absorption, then the volume change and sulfides loss will be alleviated. Thirdly, co-doped S and N can provide more sodium storage sites and enhance the conductivity of carbon tubes, thus improve the specific capacity and rate performance of MnS/NSCTs. More importantly, this method may be feasible for other anode materials, which will greatly promote the development of SIBs.

Conflicts of interest

There are no conflicts to declare.

Acknowledgements

This work was supported by the Natural Science Foundation of China (Grant No. U1804126, U1804129, 21671205, 21771164 and 21701202), Key Scientific Research Projects of Universities in Henan Province (Grant No. 19A430032 and 18A430034), Program for Interdisciplinary Direction Team in Zhongyuan University of Technology, the Collaborative Innovation Centre of Henan Textile and Clothing Industry, the Innovation Scientists and Technicians Troop Construction Projects of Henan Province (Grant No. 164100510007 and CXTD2015018).

Notes and references

1. Y. Zhang, Q. Zhou, J. Zhu, Q. Yan, S. Dou and W. Sun, *Adv. Funct. Mater.*, 2017, **27**, 1702317.
2. Q. Wang, C. Zhao, Y. Lu, Y. Li, Y. Zheng, Y. Qi, X. Rong, L. Jiang, X. Qi, Y. Shao, D. Pan, B. Li, Y. S. Hu and L. Chen, *Small*, 2017, **13**, 1701835.
3. W. Chen, X. Zhang, L. Mi, C. Liu, J. Zhang, S. Cui, X. Feng, Y. Cao and C. Shen, *Adv. Mater.*, 2019, **31**, 1806664.
4. C. Wu, Y. Jiang, P. Kopold, P. A. van Aken, J. Maier and Y. Yu, *Adv. Mater.*, 2016, **28**, 7276-7283.
5. J. Deng, W. Luo, S. Chou, H. Liu and S. Dou, *Adv. Energy Mater.*, 2017, **8**, 1701428.
6. Y. X. Wang, W. H. Lai, Y. X. Wang, S. L. Chou, X. Ai, H. Yang and Y. Cao, *Angew. Chem. Int. Ed.*, 2019, **58**, 18324-18337.
7. K. Chen, W. Zhang, Y. Liu, H. Zhu, J. Duan, X. Xiang, L. Xue and Y. Huang, *Chem. Commun.*, 2015, **51**, 1608-1611.
8. C. Dong, L. Guo, Y. He, L. Shang, Y. Qian and L. Xu, *Nanoscale*, 2018, **10**, 2804-2811.
9. J. Ni and L. Li, *Adv. Funct. Mater.*, 2018, **28**, 1704880.
10. Y. Fang, L. Xiao, Z. Chen, X. Ai, Y. Cao and H. Yang, *Electrochem. Energy Rev.*, 2018, **1**, 294-323.
11. M. Chen, W. Hua, J. Xiao, D. Cortie, W. Chen, E. Wang, Z. Hu, Q. Gu, X. Wang, S. Indris, S. L. Chou and S. X. Dou, *Nat. Commun.*, 2019, **10**, 1480.
12. M. Li, N. Muralidharan, K. Moyer and C. L. Pint, *Nanoscale*, 2018, **10**, 10443-10449.
13. Z. Xu, S. Yao, J. Cui, L. Zhou and J. K. Kim, *Energy Storage Mater.*, 2017, **8**, 10-19.
14. M. S. Balogun, Y. Luo, W. Qiu, P. Liu and Y. Tong, *Carbon*, 2016, **98**, 162-178.
15. Z. Li, J. Ding and D. Mitlin, *Acc. Chem. Res.*, 2015, **48**, 1657-1665.
16. W. Chen, S. Qi, L. Guan, C. Liu, S. Cui, C. Shen and L. Mi, *J. Mater. Chem. A*, 2017, **5**, 5332-5341.
17. S. Dong, C. Li, Z. Li, L. Zhang and L. Yin, *Small*, 2018, **14**, 1704517.
18. S. Gu, S. Wu, L. Cao, M. Li, N. Qin, J. Zhu, Z. Wang, Y. Li, Z. Li, J. Chen and Z. Lu, *J. Am. Chem. Soc.*, 2019, **141**, 9623-9628.
19. Z. Hu, Q. Liu, S. Chou and S. Dou, *Adv. Mater.*, 2017, **29**, 1700606.
20. Y. Xiao, S. Lee and Y. Sun, *Adv. Energy Mater.*, 2017, **7**, 1601329.
21. K. Chen, W. Zhang, L. Xue, W. Chen, X. Xiang, M. Wan and Y. Huang, *ACS Appl. Mater. Interfaces*, 2017, **9**, 1536-1541.
22. Y. Tan, K. W. Wong, Z. Zhang and K. M. Ng, *Nanoscale*, 2017, **9**, 19408-19414.
23. S. Qi, L. Mi, K. Song, K. Yang, J. Ma, X. Feng, J. Zhang and W. Chen, *J. Phys. Chem. C*, 2019, **123**, 2775-2782.
24. R. Hu, H. Zhao, J. Zhang, Q. Liang, Y. Wang, B. Guo, R. Dangol, Y. Zheng, Q. Yan and J. Zhu, *Nanoscale*, 2019, **11**, 178-184.
25. L. Wang, Q. Zhao, Z. Wang, Y. Wu, X. Ma, Y. Zhu and C. Cao, *Nanoscale*, 2019, **12**, 248-255.
26. S. C. Riha, A. A. Koege, X. B. Meng, I. S. Kim, Y. Q. Cao, M. J. Pellin, J. W. Elam and A. B. F. Martinson, *ACS Appl. Mater. Interfaces*, 2016, **8**, 2774-2780.
27. Y. Wang, J. Yang, S. Chou, H. Liu, W. Zhang, D. Zhao and S. Dou, *Nat. Commun.*, 2015, **6**, 8689.
28. Z. Liu, T. Lu, T. Song, X. Yu, X. Lou and U. Paik, *Energy Environ. Sci.*, 2017, **10**, 1576-1580.
29. S. Gao, G. Chen, Y. Dall'Agnese, Y. Wei, Z. Gao and Y. Gao, *Chemistry*, 2018, **24**, 13535-13539.
30. C. H. Jo, J. U. Choi and S. T. Myung, *J. Mater. Chem. A*, 2018, **6**, 6867-6873.
31. J. Zhang, H. Zhao, J. Li, H. Jin, X. Yu, Y. Lei and S. Wang, *Adv. Energy Mater.*, 2019, **9**, 1803221.
32. F. Shen, W. Luo, J. Dai, Y. Yao, M. Zhu, E. Hitz, Y. Tang, Y. Chen, V. L. Sprenkle, X. Li and L. Hu, *Adv. Energy Mater.*, 2016, **6**, 1600377.
33. Z. Zhu, F. Liang, Z. Zhou, X. Zeng, D. Wang, P. Dong, J. Zhao, S. Sun, Y. Zhang and X. Li, *J. Mater. Chem. A*, 2018, **6**, 1513-1522.
34. T. Yang, T. Qian, M. Wang, X. Shen, N. Xu, Z. Sun and C. Yan, *Adv. Mater.*, 2016, **28**, 539-545.
35. S. Kandula, K. R. Shrestha, N. H. Kim and J. H. Lee, *Small*, 2018, **14**, 1800291.
36. W. Shuang, H. Huang, L. Kong, M. Zhong, A. Li, D. Wang, Y. Xu and X. Bu, *Nano Energy*, 2019, **62**, 154-163.
37. Y. Zhang, L. Fan, P. Wang, Y. Yin, X. Zhang, N. Zhang and K. Sun, *Nanoscale*, 2017, **9**, 17694-17698.
38. R. Verma, P. N. Didwal, H.-S. Ki, G. Cao and C.-J. Park, *ACS Appl. Mater. Interfaces*, 2019, **11**, 26976-26984.
39. X. Xu, H. Zeng, D. Han, K. Qiao, W. Xing, M. J. Rood and Z. Yan, *ACS Appl. Mater. Interfaces*, 2018, **10**, 37172-37180.
40. X. Liu, K. Zhang, K. Lei, F. Li, Z. Tao and J. Chen, *Nano Research*, 2016, **9**, 198-206.
41. J. Wang, H. He, Z. Wu, J. Liang, L. Han, H. L. Xin, X. Guo, Y. Zhu and D. Wang, *J. Power Sources*, 2018, **392**, 193-199.
42. J. Li, D. Yan, X. Zhang, S. Hou, T. Lu, Y. Yao and L. Pan, *J. Mater. Chem. A*, 2017, **5**, 20428-20438.
43. X. Xu, S. Ji, M. Gu and J. Liu, *ACS Appl. Mater. Interfaces*, 2015, **7**, 20957-20964.
44. X. Gao, X. Zhang, J. Jiang and J. Chen, *Mater. Lett.*, 2018, **228**, 42-45.
45. S. H. Chaki, M. P. Deshpande, J. P. Tailor, K. S. Mahato and M. D. Chaudhary, *Adv. Mater. Research*, 2012, **584**, 243-247.
46. Y. Tang, T. Chen, W. Guo, S. Chen, Y. Li, J. Song, L. Chang, S. Mu, Y. Zhao and F. Gao, *J. Power Sources*, 2017, **362**, 1-9.
47. A. Sumboja, C. Y. Foo, X. Wang and P. S. Lee, *Adv. Mater.*, 2013, **25**, 2809-2815.
48. D. T. Pham, T. T. Vu, S. Kim, B. Sambandam, V. Mathew, J. Lim and J. Kim, *Adv. Energy Mater.*, 2019, **9**, 1900710.
49. X. Yu and A. Manthiram, *J. Phys. Chem. Lett.*, 2014, **5**, 1943-1947.
50. B. Liu, Z. Liu, D. Li, P. Guo, D. Liu, X. Shang, M. Lv and D. He, *Appl. Surf. Sci.*, 2017, **416**, 858-867.
51. M. Wan, Y. Tang, L. Wang, X. Xiang, X. Li, K. Chen, L. Xue, W. Zhang and Y. Huang, *J. Power Sources*, 2016, **329**, 290-296.
52. Y. Ma, Y. Ma, D. Bresser, Y. Ji, D. Geiger, U. Kaiser, C. Streb, A. Varzi and S. Passerini, *ACS Nano*, 2018, **12**, 7220-7231.
53. X. Xu, J. Liu, J. Liu, L. Ouyang, R. Hu, H. Wang, L. Yang and M. Zhu, *Adv. Funct. Mater.*, 2018, **28**, 1707573.
54. M. Hou, Y. Qiu, G. Yan, J. Wang, D. Zhan, X. Liu, J. Gao and L. Lai, *Nano Energy*, 2019, **62**, 299-309.

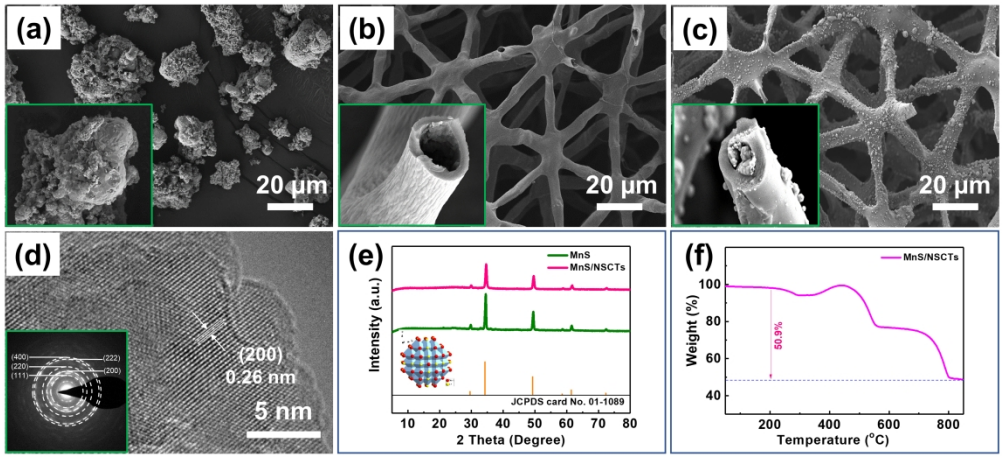

Fig. 1 Morphologies of the samples. (a) SEM image of MnS; (b) SEM image of the carbon tubes; (c) SEM image of MnS/NSCTs; (d) TEM image and SAED of MnS/NSCTs; (e) XRD patterns; (f) TG curves.

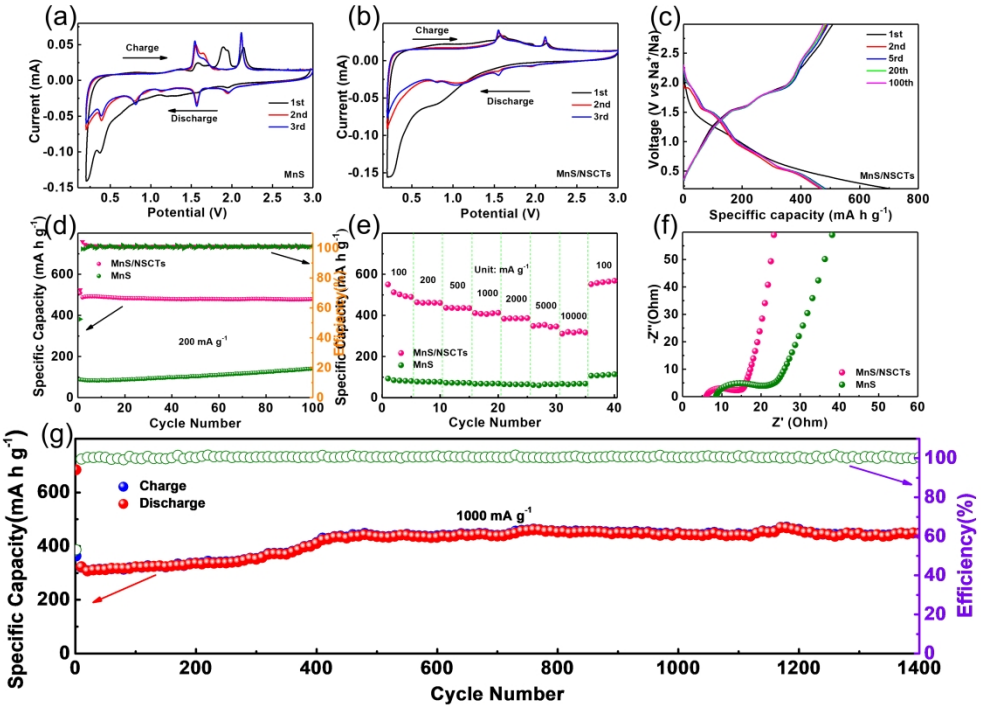

Fig. 2 Electrochemical performance of the samples (the voltage range is 0.2~3.0 V, and the specific capacities are based on the weight of MnS or MnS/NSCTs samples). (a) CV curves of MnS; (b) CV curves of MnS/NSCTs; (c) charge-discharge profiles of MnS/NSCTs; (d) cycle contrast; (e) rate contrast; (f) EIS contrast; (g) long cycle performance of MnS/NSCTs.

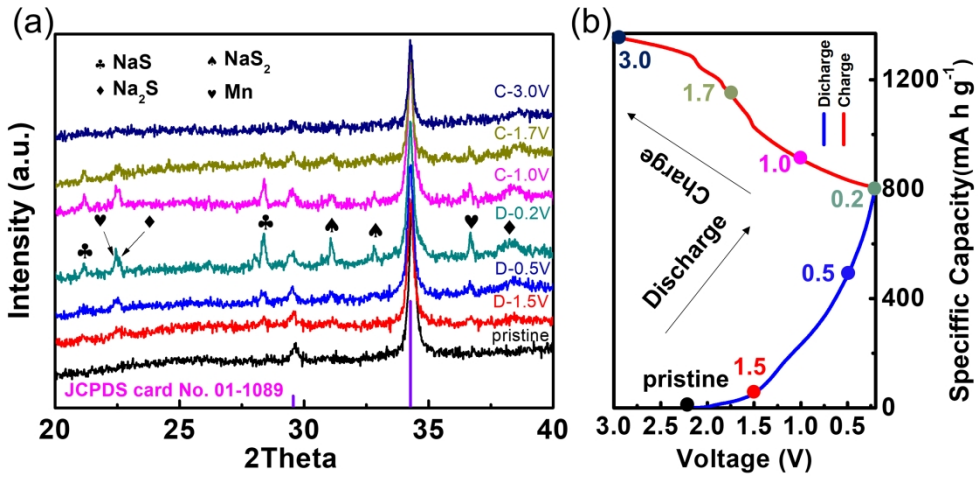

Fig. 3 Crystal structure evolution of MnS/NSCTs during the sodium storage process. (a) ex-situ XRD patterns; (b) corresponding charge-discharge profiles.

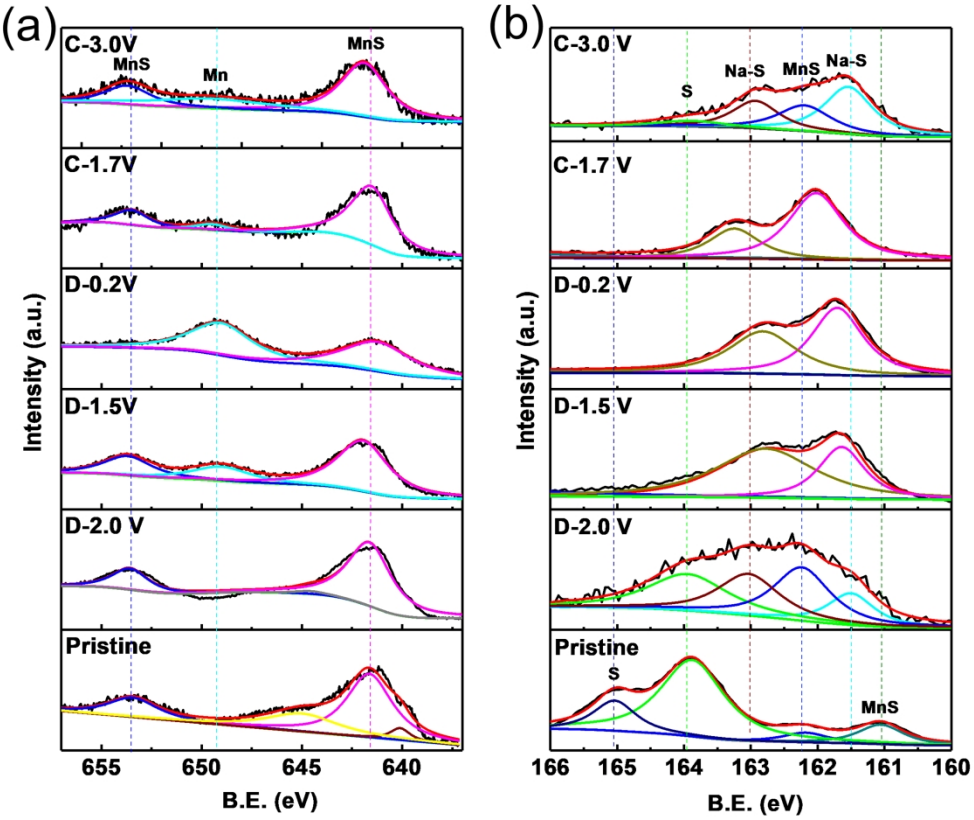

Fig. 4 Chemical component evolution of MnS/NSCTs during the sodium storage process. (a) XPS spectrum of Mn; (b) XPS spectrum of S.

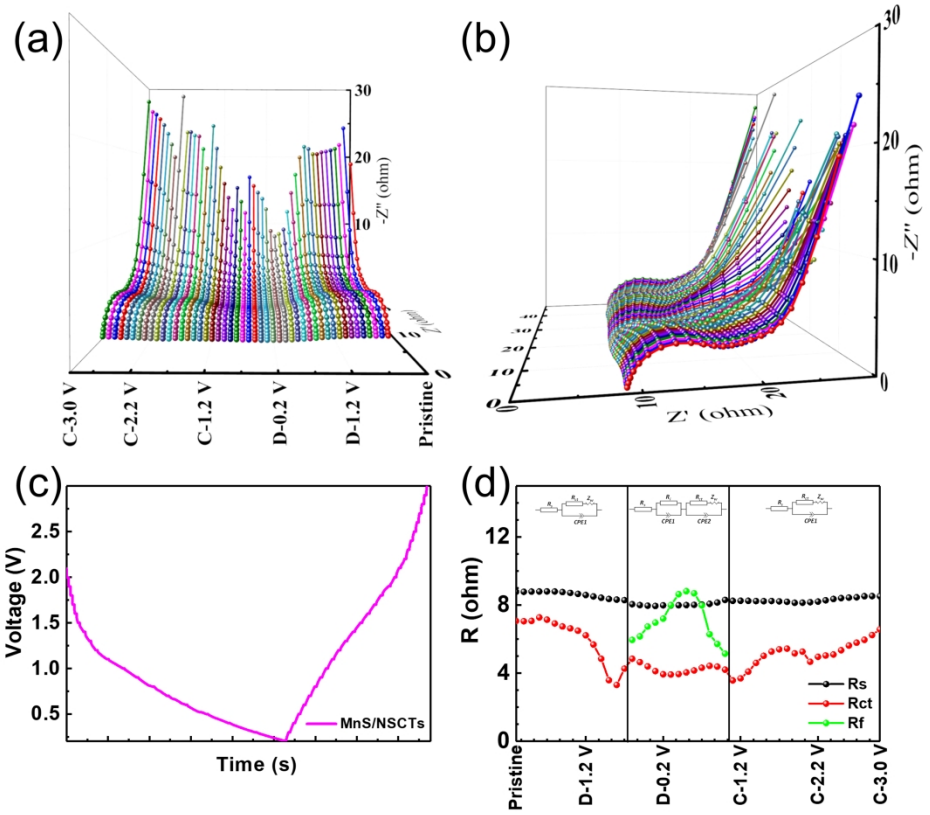

Fig. 5 EIS evolution of MnS/NSCTs during the sodium storage process. (a) (b) EIS curves evolution; (c) corresponding charge-discharge profiles; (d) resistance value evolution according to equivalent circuit fitting.

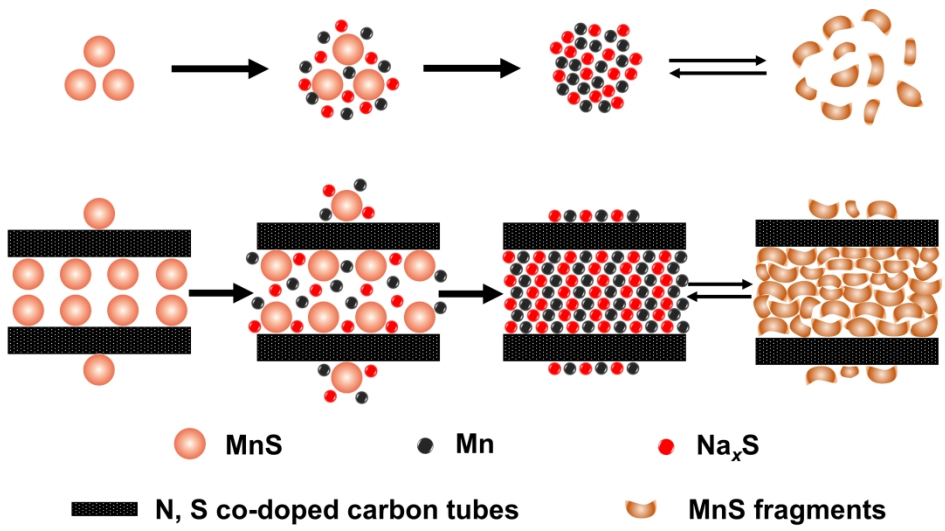

Fig. 6 Micro-structure evolution contrast between MnS and MnS/NSCTs during the sodium storage process.

Table of Contents Entry

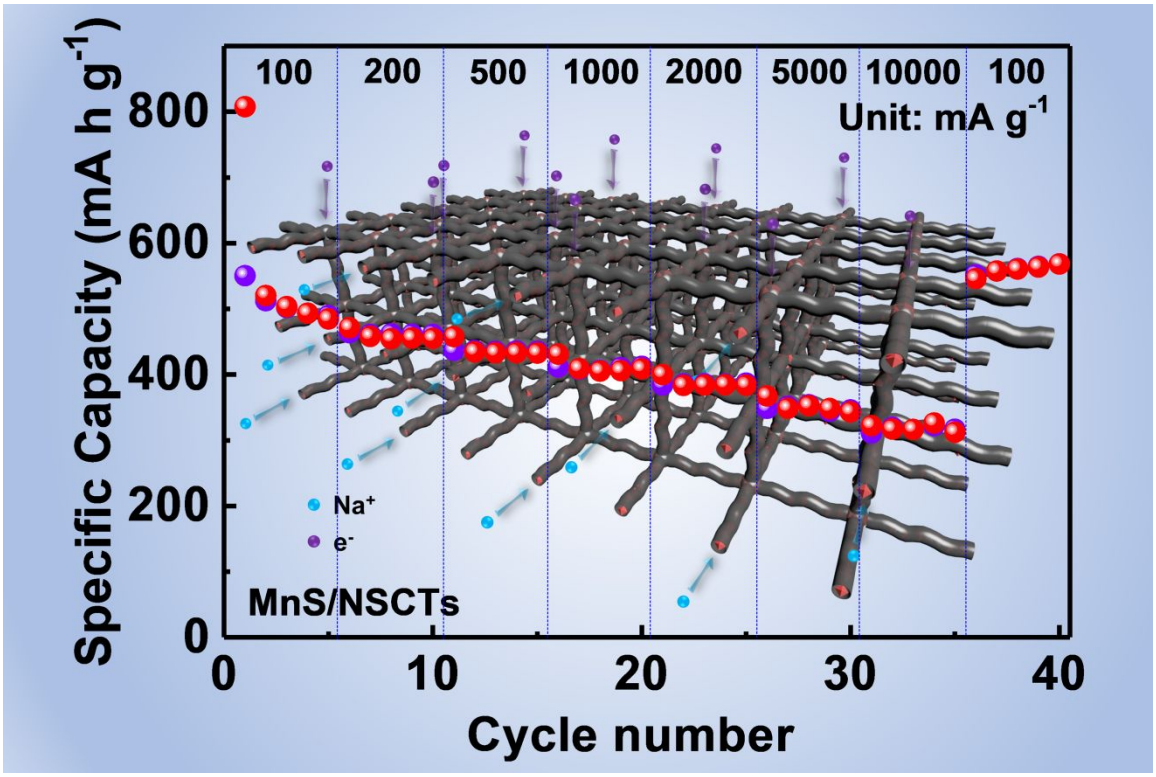

Inspired by common cream rolls, MnS/N, S co-doped carbon tubes composite with 3D cross-linked tubular structure is prepared via a simple and low-cost method. This cream rolls-like composite delivers the best comprehensive electrochemical performance until now among all MnS electrodes for sodium-ion batteries. Besides, the conversion reaction mechanism of MnS/N, S co-doped carbon tubes is clearly revealed by several *in-situ* and *ex-situ* techniques.

Electronic Supplementary Information

Cream rolls-inspired advanced MnS/C composite for sodium-ion batteries: Encapsulating MnS creams into hollow N, S co-doped carbon rolls

Gaojie Li,[a] Kongyao Chen,*[a] Yanjie Wang,[a] Zhuo Wang,[a] Xueli Chen,[a] Siwen Cui,[a] Zijie Wu,[a,c] Constantinos Soutis,[c] Weihua Chen,*[b] Liwei Mi*[a]

[a] *Center for Advanced Materials Research, Zhongyuan University of Technology, Henan 450007, P. R. China*

[b] *College of Chemistry and Molecular Engineering, Zhengzhou University, Henan 450001, P. R. China*

[c] *The University of Manchester Aerospace Research Institute, University of Manchester, Manchester M13 9PL, United Kingdom*

* Corresponding author: *mlwzzu@163.com, chenweih@zzu.edu.cn, chenkongyao@zut.edu.cn.*

Experimental Section

Preparation of MnS/NSCTs composites. MnS/NSCTs composites were prepared by a simple freeze drying and heat treatment method. Firstly, 1.2 g $Mn(CH_3COO)_2{\cdot}4H_2O$ and 0.5 g cetyl trimethyl ammonium bromide (CTAB) were dissolved completely into 50 mL distilled water. Then, 1.0 g juncus was immersed into the solution and dried at 60°C overnight. After that, the precursor is freezed and dried for 24 h in a freeze dryer, then calcinated at 700°C for 5 h with the protection of N_2. Lastly, the samples were mixed with sulfur (weight ratios of 1:10) and calcinated at 500°C for 3 h with the protection of N_2, then MnS/NSCTs composites were achieved. Pure MnS are prepared via a similar way without the presence of juncus.

Material characterization. X-ray diffraction (XRD) and *ex-situ* XRD patterns were obtained with Polycrystalline X-ray powder diffractometer (Ultima IV, Rigaku Corporation) with Cu-Kα radiation. The microstructures and energy dispersive X-ray maps were obtained by scanning electron microscopy (SEM, Zeiss Merlin Compact). X-ray photoelectron spectroscopy (XPS) and *ex-situ* XPS analysis was performed by an energy spectrometer (Thermo Scientific K-Alpha) Thermogravimetric (TG) analysis was obtained by a thermo analyzer (TG 209F1, NETZSCH) from 50 to 850°C with a heating rate of 10°C min^{-1} in air. The specific surface area and pore distribution were calculated by Barrett-Joyner-Halenda (BJH) method.

Electrochemical Measurements. MnS/NSCTs electrodes were prepared by mixing MnS/NSCTs composites, acetylene black, and Polyvinylidene Fluoride (PVDF) with a weight ratio of 7:2:1, and 1-methyl-2-pyrrolidone was selected as the

solvent. Then the slurry was uniformly coated onto a copper foil, and dried at 80°C for 8 h. After rolled by a roller press, the copper foil was cut into wafers with a diameter of 8 mm. The mass loading of the active material was about 1~2 mg cm^{-2}. The working electrodes were MnS/NSCTs electrodes, the counter electrodes were home-made Na slices, the electrolyte was 1 mol L^{-1} sodium trifluomethanesulfonate in diethylene glycol dimethyl ether ($NaCF_3SO_3$/DEGDME), and the separators were glass fiber filters (Whatman GF/D). Then CR-2032 coin cells were assembled in an Ar filled glove box. The galvanostatic charge-discharge test was carried out by a multichannel battery tester (LAND CT2001A, Wuhan), and all the specific capacities are based on the weight of MnS/NSCTs composite. The voltage range is 0.2~3.0 V, and the specific capacity is based on the total mass of MnS or MnS/NSCTs samples. The cyclic voltammetry (CV) test was performed by an electrochemical workstation (CHI 660e, chenhua, Shanghai), and the scan rate was 0.2 mV s^{-1} with a voltage range of 0.2~3 V. Electrochemical impedance spectrum (EIS) and *in-situ* EIS was performed by an electrochemical workstation (Zennium-pro, Germany, Zahner), and the frequency range was from 0.1 Hz to 100 kHz.

BET Results

The specific surface area and pore size distribution of MnS/NSCTs composite are investigated by BET test. In Fig. 2b, the isothermal absorption-desorption curves of MnS/NSCTs manifest an IV-type absorption isothermal feature[1, 2]. According to the pore size distribution, MnS/NSCTs sample shows a typical mesoporous feature with a specific surface area of 36.05 m^2 g^{-1}, and the average porous size is 3.74 nm. However, numerous cavities in the tubes may not be detected by BET because of their oversize diameter (2~4 μm).

TG Results

TG is performed to ascertain the component of MnS/NSCTs. As is shown in Fig. 2c, the little weight loss below 200°C is attributed to the evaporation of water in the sample. Whereafter, slight weight increase appears from 340°C to 400°C, which may result from the formation of Mn_3O_4 and $MnSO_4$. The weight loss between 420°C and 520°C corresponds to the oxidization of carbon tubes, and the weight loss between 600°C and 800°C may come from the formation of Mn_2O_3. According to the TG curve, the weight ratio of MnS is about 56.0% in the cream roll-like MnS/NSCTs sample.

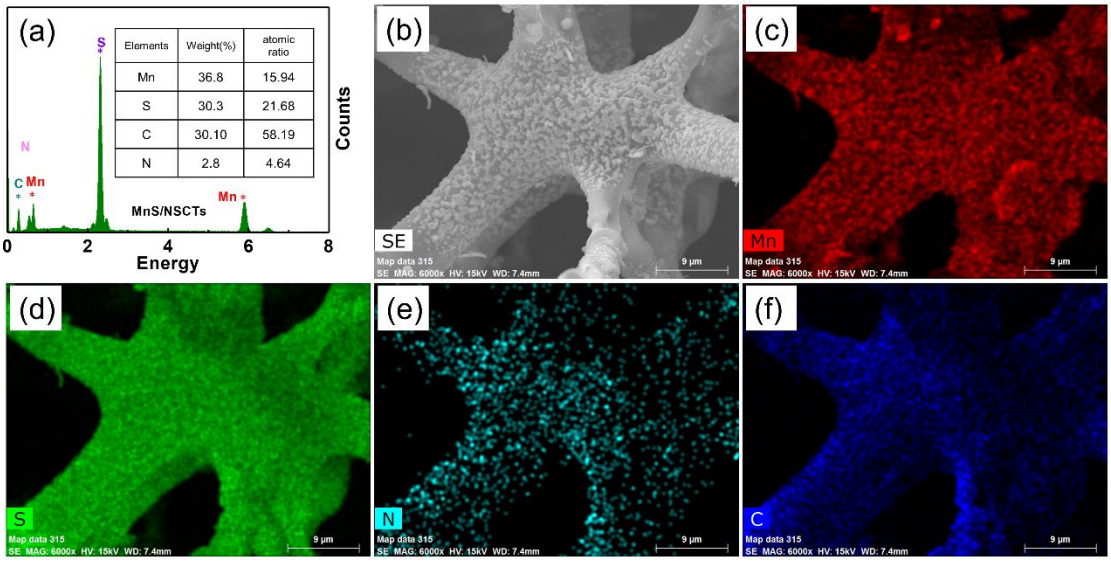

Fig. S1 Element analysis of MnS/NSCTs. (a) EDX; (b) morphology; (c) (d) (e) (f) mapping images of Mn, S, N and C.

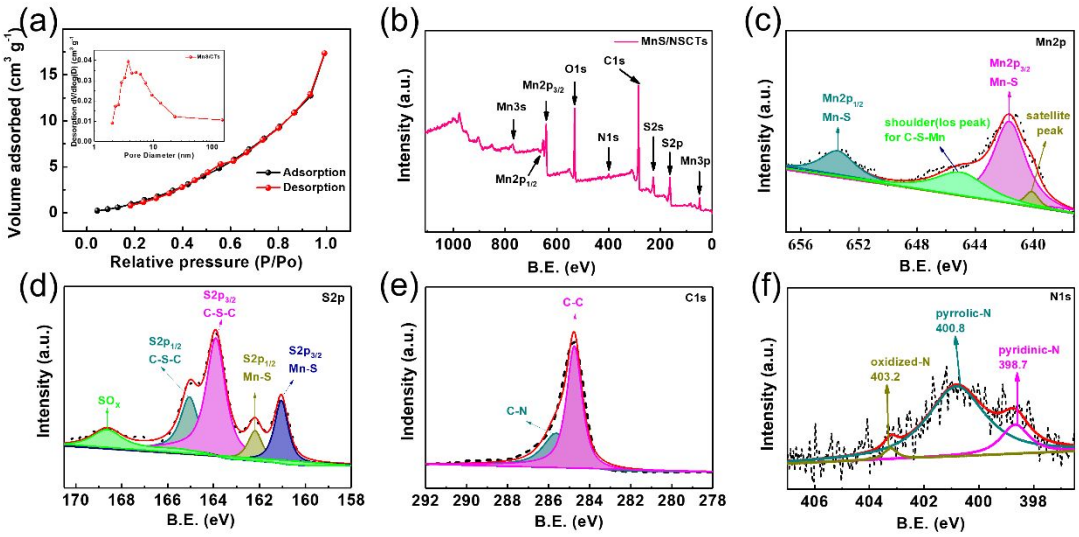

Fig. S2 BET and XPS of MnS/NSCTs. (a) Nitrogen adsorption-desorption curves and pore size distributions; (b) survey XPS spectrum of MnS/NSCTs; (c) (d) (e) (f) high-resolution XPS spectra of Mn, S, C and N. (a) XPS survey spectrum of MnS/NSCTs; (b) N1s spectrum of MnS/NSCTs.

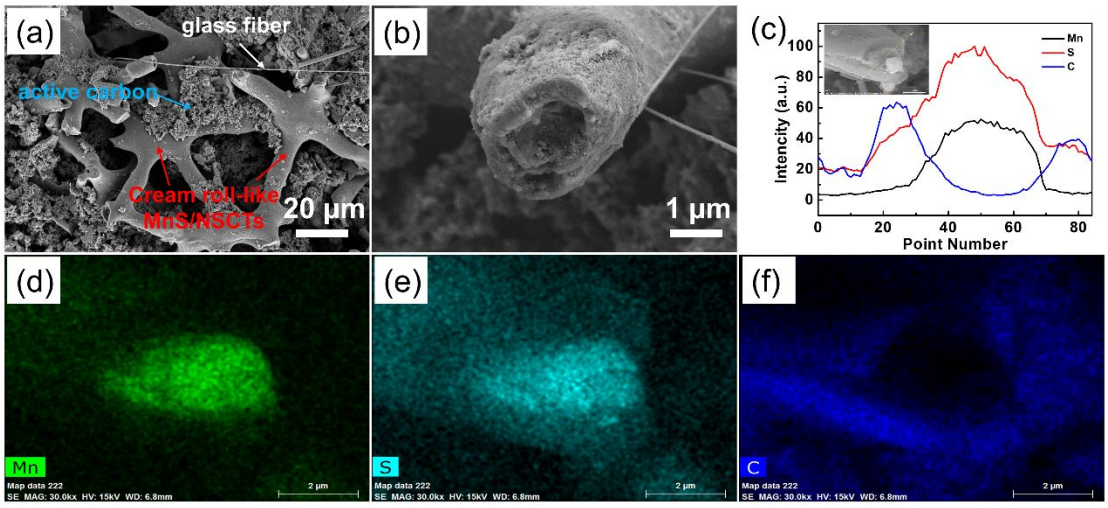

Fig. S3 Morphology and element distribution of MnS/NSCTs after 100 cycles. (a) (b) SEM images; (c) line scan results; (d) (e) (f) mapping images of Mn, S and C.

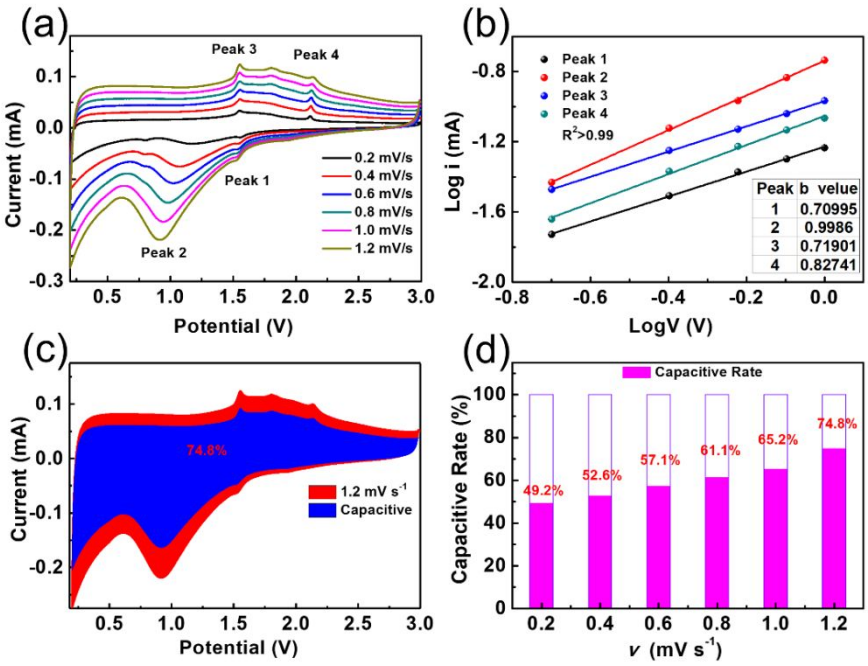

Fig. S4 CV test of MnS/NSCTs at various scan rates. (a) CV curves; (b) relationship of log *i* vs. log *v*; (c) capacitive capacity contribution at 1.2 mV s-1; (d) capacitive capacity contribution at various scan rates.

References

1. S. Gao, G. Chen, Y. Dall'Agnese, Y. Wei, Z. Gao and Y. Gao, *Chemistry - A European Journal*, 2018, **24**, 13535-13539.
2. X. Xu, H. Zeng, D. Han, K. Qiao, W. Xing, M. J. Rood and Z. Yan, *ACS Appl. Mater. Interfaces*, 2018, **10**, 37172-37180.